Quantum Information Processing (2025) 24:325
https://doi.org/10.1007/s11128-025-04947-8

Exploring the use of quantum computers for resilience analysis in critical infrastructure networks

Christoph Brockt-Haßauer[1] · Vyacheslav Shatokhin[2,3] · Aishvarya Kumar Jain[1] · Corinna Köpke[1] · Alexander Stolz[1] · Mirjam Fehling-Kaschek[1] · Andreas Buchleitner[2,3]

Received: 8 August 2024 / Accepted: 20 September 2025

Abstract
Resilience analysis of networks representing critical infrastructure is a computationally hard problem, and the question arises of whether quantum computers may be beneficial for this purpose. On the way towards an answer to this problem, we map a small critical infrastructure network on a quantum network composed of dipole–dipole-coupled nodes. The latter are each equipped with up to three discrete (quantum) states, two of which support the connectivity of the network, while the third state, reachable through nondeterministic spontaneous processes, represents a 'broken' node. A finite 'repair' time is needed to restore the node. To study the dynamics of such networks on a quantum computer, we derive unitary dilations of Kraus operators governing the evolution of our open quantum network, and generate corresponding quantum circuits using the `qiskit` interface. We then study the population dynamics of several cases of increasing complexity on the quantum hardware. We discuss how scaling of errors is related to the depth of the quantum circuits. Ultimately, we show that open quantum systems can be used for modelling critical infrastructure, but quantum computers with much lower error rates than currently available are required for a quantitative resilience analysis.

Keywords Quantum computing · Open quantum systems · Resilience · Quantum networks

Christoph Brockt-Haßauer and Vyacheslav Shatokhin have contributed equally to this work.

✉ Christoph Brockt-Haßauer
christoph.brockt-hassauer@emi.fraunhofer.de

[1] Fraunhofer Institut für Kurzzeitdynamik, Ernst-Mach-Institut, EMI, Ernst-Zermelo-Str. 4, 79104 Freiburg, Germany

[2] Physikalisches Institut, Albert-Ludwigs-Universität Freiburg, Hermann-Herder-Str. 3, 79104 Freiburg, Germany

[3] EUCOR Centre for Quantum Science and Quantum Computing, Albert-Ludwigs-Universität Freiburg, Hermann-Herder-Str. 3, 79104 Freiburg, Germany

Published online: 03 October 2025

1 Introduction

Critical infrastructures, such as gas or power supply networks, play a crucial role in economics and for the well-being of modern societies. Any disruption of such infrastructure, either man-made or natural, can lead to significant damage. Therefore, resilience analysis of critical infrastructure is an important research area, and powerful classical simulation techniques have been developed for this purpose [1–3]. With the help of such simulations, the impact of different kinds of events on the infrastructure can be quantified and different mitigation strategies can be evaluated [4, 5].

Commonly, critical infrastructure is described using a network-based approach: All relevant components of the infrastructure are represented by nodes that are interlinked by the arcs of the network. Before a disruption event, the network exhibits its maximal performance. A failure of one node or arc at some time may lead to a cascade of damages inside the critical infrastructure network, resulting in a substantial drop of the network's performance. Apart from disruptions, network models also incorporate the nodes' ability to be repaired and to restore their functionality after a characteristic time. A simulation is set up as a time-resolved evaluation of the network's status, by monitoring the network's performance, e.g. measured as the percentage of working components as a function of time. The network's resilience can then be evaluated from the performance integrated over time.

Both the rapid increase in a network's complexity with the number of nodes and arcs and the consideration of a large number of possible incidents and their outcome pose severe challenges to classical computers for sound resilience analyses. Since quantum computers (QC), once realized in practice, will be able solve a number of computationally hard problems, from simulation of quantum systems [6] to factorization of large numbers [7] to unstructured database searches [8], a natural question arises as whether gate-based QC can also be beneficial in resilience analysis of finite networks representing critical infrastructure. This question can be split into two parts: (1) how to map a finite classical network representing critical infrastructure onto a corresponding quantum network whose dynamics can be studied on a QC, and (2) how to identify, using a QC, a configuration (topology) of the network that is most resilient in the presence of disruptions? This paper deals with the first part of this problem.

In the following, we present a small three-node quantum network as a minimal model of critical infrastructure and justify why its nodes are modelled as three-level open quantum systems. We then move on, step by step, from the master equation governing the network's dynamics, over the Kraus representation thereof, to the unitary dilation of the Kraus operators and to the implementation of the simulation on a gate-based QC. We report on our experience with the IBM Q System One in Ehningen [9] for four cases of increasing complexity and show how rapidly the results of quantum simulations lose their accuracy for a relatively simple network.

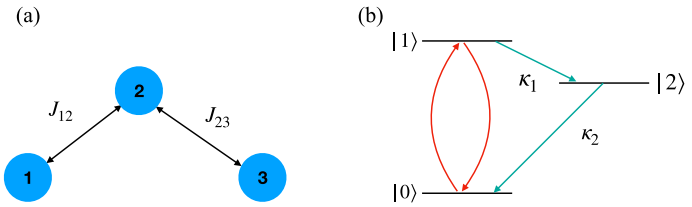

Fig. 1 **a** Three-node network with nodes (blue circles) connected by internodal links with coupling strengths J_{ij} (double-sided arrows). **b** Each node is a three-level system, whose levels $|0\rangle$ and $|1\rangle$ represent qubit states that can be controlled by unitary operations. Level $|2\rangle$ is a 'defect' state modelling node's 'damage' (via the transition $|1\rangle \rightarrow |2\rangle$, with rate κ_1). Via the transition $|2\rangle \rightarrow |0\rangle$, with rate κ_2, a damaged node can be repaired. The damage and repair processes are described as non-unitary operations

2 Quantum network model of critical infrastructure

2.1 Quantum system

Let us consider a simple classical network with three nodes 1, 2 and 3 that are connected by two links, characterized by the coupling strengths J_{12} and J_{23}, as shown in Fig. 1a. In the ideal case of a functional network, it can feature a flow, e.g. of electric current between the nodes. To describe an infrastructure, whose resilience we would like to analyse, also damage and repair need to be incorporated in the model. For simplicity, we assume that disruption events can directly lead to failure solely of nodes. Thereby, the links are affected indirectly: if one of the nodes fails it falls out of the network; as a result, one or two links connecting it with other nodes are also damaged.

When we translate this qualitative description of the network into the quantum language, then the fully functional network can be associated with three two-level quantum systems (nodes) that are coupled with each other by the dipole–dipole-type interactions (links) which describe the flip-flop of excitations between states of distinct nodes. Such quantum networks are ubiquitous in studies of efficient energy transport in energy harvesting systems [10–12]. However, modelling of nodes as two-level systems does not allow to describe the inclusion of nodes' damage. For that purpose, we furnish nodes with an additional 'defect' level; hence our model of the node as a three-level quantum system, see Fig. 1b. Such nodes can be physically realized using atoms, ions or other quantum systems that are employed as platforms for quantum computations [13]. States $|0\rangle$ and $|1\rangle$ of the nodes are qubit levels that can be manipulated coherently (unitarily), e.g. by laser pulses, while state $|2\rangle$ is a meta-stable level [14, 15] that serves to model the node's damage. We describe damage as an incoherent (non-unitary) process transferring the node from state $|1\rangle$ to state $|2\rangle$, with rate κ_1. Correspondingly, a damaged node can be repaired by bringing it from state $|2\rangle$ to state $|0\rangle$, with rate κ_2. The presence of non-unitary processes qualifies our network as an open quantum system [16].

We will now present in more detail the unitary processes pertinent to our network and describe the non-unitary part in the following section. The unitary evolution of the network is generated by Hamiltonian operators. The interaction of node α with the

external field can be described by the Hamiltonian $H_\alpha = \hbar\Omega(t)[\sigma_{01}^\alpha + \sigma_{10}^\alpha]$, where $\Omega(t)$ is the Rabi frequency and $\sigma_{ij}^\alpha = |i\rangle_\alpha\langle j|_\alpha$ are the dipole transition operators. The pairwise dipole–dipole interaction Hamiltonian is given by (henceforth, we for brevity omit the identity operators for the nodes excluded from the interactions)

$$H_{\text{int}} = \hbar \sum_{\alpha=1}^{2} J_{\alpha,\alpha+1}(\sigma_{01}^\alpha \sigma_{10}^{\alpha+1} + \sigma_{10}^\alpha \sigma_{01}^{\alpha+1}). \tag{1}$$

A general mixed state of such a three-node quantum network can be described by a density operator $\rho(t)$. The latter belongs to the space of linear operators acting upon the Hilbert space of three nodes, $\mathcal{H} = \mathcal{H}_1 \otimes \mathcal{H}_2 \otimes \mathcal{H}_3$, where $\mathcal{H}_\alpha$ is the Hilbert space of node α spanned by vectors $\{|0\rangle, |1\rangle, |2\rangle\}_\alpha$; thus, $\dim \rho(t) = 3^3 \times 3^3 = 27 \times 27$, with basic vectors $\{|0,0,0\rangle, |0,0,1\rangle, \ldots, |2,2,2\rangle\}$, where $|i,j,k\rangle := |i\rangle_1 \otimes |j\rangle_2 \otimes |k\rangle_3$.

2.2 Network dynamics

2.2.1 Master equation

We postulate that the network's density operator $\rho(t)$ obeys a Lindblad master equation, which can be derived in open quantum systems theory under the Born–Markov approximation [16]:

$$\dot{\rho}(t) = -\frac{i}{\hbar}[H, \rho(t)] - \sum_{\alpha=1}^{3}\sum_{k=1}^{2}(L_{k\alpha}^\dagger L_{k\alpha}\rho(t) + \rho(t)L_{k\alpha}^\dagger L_{k\alpha} - 2L_{k\alpha}\rho(t)L_{k\alpha}^\dagger). \tag{2}$$

In (2), the Hamiltonian H reads

$$H = H_{\text{F}} + H_{\text{int}}, \tag{3}$$

where $H_{\text{F}} = H_1 + H_2 + H_3$ is the Hamiltonian operator describing the interaction of the individual nodes' qubit levels with the external fields, and $L_{k\alpha}$ are the Lindblad (or jump) operators whose subscripts $k \in \{1, 2\}$ label damage and repair processes. The jump operators read

$$L_{1\alpha} = \sqrt{\kappa_{1\alpha}}\sigma_{21}^\alpha, \quad L_{2\alpha} = \sqrt{\kappa_{2\alpha}}\sigma_{02}^\alpha. \tag{4}$$

For Eq. (2), we also use the shorthand notation $\dot{\rho}(t) = \mathcal{L}\rho(t)$, with $\mathcal{L}$ being the Liouvillian. Additionally, we drop the subscript α for κ_1 and κ_2, and we will consider networks with only one three-level node in our QC experiments below. (The other two nodes will be modelled as 'defect-free' two-level systems.) Clearly, because of the presence of the Lindblad operators on the r.h.s. of (2), the evolution of the density operator, $\rho(t) = e^{\mathcal{L}t}\rho(0)$ is non-unitary.

A simulation of a non-unitary evolution on a quantum computer presents a certain challenge, and a lot of attention in recent years has been dedicated to this problem

[17–22]. We adhere to the method whose basic idea is to embed an open quantum system into a larger Hilbert space [23]. The prerequisite for such an embedding is the Kraus, or operator-sum representation of $\rho(t)$ [13]:

$$\rho(t) = \sum_n M_n(t)\rho(0)M_n^\dagger(t), \quad \sum_n M_n^\dagger(t)M_n(t) = \mathrm{id}, \tag{5}$$

where $M_n(t)$ is a Kraus operator and id is the identity operator, with dimension $\dim(\mathrm{id}) = \dim(\rho(t))$.

2.2.2 Kraus operators

For an effective implementation of unitary extensions of the Kraus operators on a quantum computer, it is useful to solve (2) in an analytical form. Therefrom one can derive the Kraus operators $M_n(t)$, for example, via the recipe proposed in [24].

According to [24], one first needs to find the spectral decompositions of the $N \times N$-dimensional density operators, $\rho(0)$ and $\rho(t)$, respectively,

$$\rho(0) = \sum_{n=1}^{N} p_n(0)|\psi_n(0)\rangle\langle\psi_n(0)|, \tag{6}$$

$$\rho(t) = \sum_{n=1}^{N} p_n(t)|\psi_n(t)\rangle\langle\psi_n(t)|, \tag{7}$$

where $|\psi_n(0)\rangle$ ($|\psi_n(t)\rangle$) and $p_n(0)$ ($p_n(t)$) are orthonormal eigenvectors and corresponding eigenvalues of the density operator $\rho(0)$ ($\rho(t)$).

Using the N eigenvalues of $\rho(t)$, one constructs N matrices of dimension $N \times N$, $M_0'(t), \ldots, M_{N-1}'(t)$, as follows:

$$M_0'(t) = \begin{pmatrix} \sqrt{p_1(t)} & 0 & \ldots & 0 \\ 0 & \sqrt{p_2(t)} & \ldots & 0 \\ \ldots & \ldots & \ldots & \ldots \\ 0 & 0 & \ldots & \sqrt{p_N(t)} \end{pmatrix}, \tag{8}$$

$$\ldots$$

$$M_{N-1}'(t) = \begin{pmatrix} 0 & \ldots & 0 & \sqrt{p_1(t)} \\ \sqrt{p_2(t)} & \ldots & 0 & 0 \\ \ldots & \ldots & \ldots & \ldots \\ 0 & \ldots & \sqrt{p_N(t)} & 0 \end{pmatrix}. \tag{9}$$

In words, as the subscript $n = 0, 1, \ldots, N-1$ of the matrix $M_n'(t)$ increases by one, the nonzero entries in each row, given by the square roots of the eigenvalues $\sqrt{p_1(t)}, \ldots, \sqrt{p_N(t)}$, are shifted one position rightwards (modulo N). Finally, from Eqs. (6), (7), (8) and (9), the Kraus operators are given by

$$M_n(t) = V(t)M_n'(t)V(0)^\dagger, \quad n = 0, \ldots, N-1, \tag{10}$$

where $V(t)$ is the unitary matrix whose columns are the eigenvectors of $\rho(t)$:

$$V(t) = (|\psi_1(t)\rangle, \quad |\psi_2(t)\rangle, \quad \ldots, \quad |\psi_N(t)\rangle). \tag{11}$$

We note that the Kraus representation obtained in this way depends not only on the operator structure of (2), but also on the initial state $\rho(0)$.

We verified the above algorithm by applying it to a single three-level system (a single node of our network) with two decay channels. In this case, an exact operator solution of the corresponding master equation (obtained from (2) with single-valued $\alpha = 1$) is known [25]. To make a closer connection to other cases studied in the present contribution (see Sect. 4), we considered an initially excited node in state $|1\rangle$ and the absence of continuous driving. This condition suggests a representation (we drop superscript 1 for simplicity) $H_F = \pi\delta(0)[\sigma_{01} + \sigma_{10}]$, where $\delta(x)$ is the Dirac delta function, that is, a delta impulse with the pulse area π acting on the node in its state $|0\rangle$ at $t = 0$, and exciting it to state $|1\rangle$. Although the operator solution of [25] and the method of [24] result in distinct matrix representations of the Kraus operators, both representations yield equivalent evolutions of the density matrix.

Next, we considered more complicated networks that are composed of several nodes coupled by the dipole–dipole interactions, and yet simple enough, such that we could obtain the spectral decompositions (6) and (7) in an analytical form. To that end, again, we restricted the state space of our network to the single excitation subspace, which allowed for derivation of analytical expressions. Furthermore, we focused on networks including only one damageable node, coupled to one or two two-level systems (that is, ideal nodes without the defect level), which further reduces the (effective) dimension of the network's state space. More precisely, for two-node networks (compounded of nodes 1 and 2), the effective Hilbert space $\mathcal{H}_{\text{eff}}$ is four-dimensional, spanned by the vectors $\{|0, 0\rangle, |0, 1\rangle, |1, 0\rangle, |2, 0\rangle\}$; and in the case of three nodes, it is five-dimensional, spanned by the vectors $\{|0, 0, 0\rangle, |0, 0, 1\rangle, |0, 1, 0\rangle, |1, 0, 0\rangle, |2, 0, 0\rangle\}$. For two nodes, we obtained the Kraus operators in symbolic form for arbitrary parameter values, while for three nodes, these operators were derived in an analytical form as functions of time by fixing the numerical values of $J_{12} = J_{23} =: J$ and of κ_1, κ_2 (see Appendix A). We checked that $M_n(t)$ always satisfies Eq. (5).

2.2.3 Unitary dilation

In order to be able to simulate open quantum systems on quantum computers, it is necessary to find a representation of the system dynamics including unitary operators alone. Given the Kraus operators (10), their unitary extensions can be obtained by several techniques, for example, by Richardson's extrapolation [20]. In our work, we have implemented another method that is based on Szőkefalvi-Nagy's dilation theorem [26], which was used to simulate the spontaneous emission of a single two-level atom on a QC [17].

The useful property of Sz.-Nagy's dilation is its linear scaling with the dimension of Kraus operators: for a Kraus operator M_n having dimension $d \times d$, its unitary dilation's dimension is dim $U_n = 2d \times 2d$. The unitary operator $U_n(t)$ is constructed

as follows [26]:

$$U_n(t) = \begin{pmatrix} M_n(t) & (\mathrm{id} - M_n(t)M_n^\dagger(t))^{1/2} \\ (\mathrm{id} - M_n^\dagger(t)M_n(t))^{1/2} & -M_n^\dagger(t) \end{pmatrix}. \tag{12}$$

Before the evolution of an open quantum system can be studied on a quantum computer, the dimension of $U_n(t)$ may need to be expanded to match the dimension of an integer number of qubits. For example, for the three-node network that is spanned by the five-dimensional Hilbert space specified above in Sect. 2.2.2, $\dim\{U_n(t)\} = 10 \times 10$. Thus, four qubits spanning a 16-dimensional Hilbert space are required to simulate such network. It is easy to show that in the general case, a quantum network consisting of N three-level nodes can be represented by M qubits, where M scales linearly with N:

$$M \geq 1 + N\frac{\log(3)}{\log(2)}. \tag{13}$$

The matrices $U_n(t)$ are transformed to 16×16-dimensional ones, $\tilde{U}_n(t)$, by appending to them 6×6-dimensional identity matrices as diagonal blocks and padding the off-diagonal blocks with zeros. Then, the initial density operator $\rho(0)$ is decomposed in terms of pure states, $\rho(0) = \sum_k c_k|\varphi_k\rangle\langle\varphi_k|$. (In our case, only one of the nodes is initially excited, such that $\rho(0)$ is already pure and the sum reduces to a single term with $k = 1$ and $c_1 = 1$.) In matrix representation, the initial state $|\varphi_1\rangle = |1, 0, 0\rangle$ corresponds to a five-dimensional vector $\vec{v} = (0, 1, 0, 0, 0)^T$. We extend $\vec{v}$ to a 16-dimensional vector $\tilde{\vec{v}}$ by appending to it an 11-dimensional null vector.

Now, for every n, the unitary evolutions, $\tilde{U}_n(t)\tilde{\vec{v}}$, can be implemented on a quantum computer, as detailed in Sect. 3.

2.3 Relation to critical infrastructure networks

The toy quantum network introduced in Sect. 2.2.1 incorporates essential properties of critical infrastructure networks that are required for the latter's realistic simulation. The most important feature is that nodes can be damaged and repaired. For the resilience analysis, the performance loss of the system under study needs to be quantified for given threats. In its simplest form, the resilience analysis of a critical infrastructure network includes simulation of the time evolution of the network components and tracking the percentage of working nodes, see exemplary Fig. 2. A single-valued resilience indicator can be obtained from the integrated performance loss.

In a classical simulation, a certain damage probability, p_d, and a mean time to repair, t_r, are assigned to the nodes. These quantities in a quantum network can be adjusted by varying the excitation rate of level $|1\rangle$ and the rates κ_1 and κ_2, such that the steady-state population of level $|2\rangle$ coincides with the probability of the node being damaged in the classical simulation. Thus, our quantum model offers the opportunity to simulate a minimal network with node damage and repair. By real-time simulation of quantum jumps [16] in a quantum network, it is possible to generate the evolution of performance versus time that is reminiscent of the corresponding classical curves in

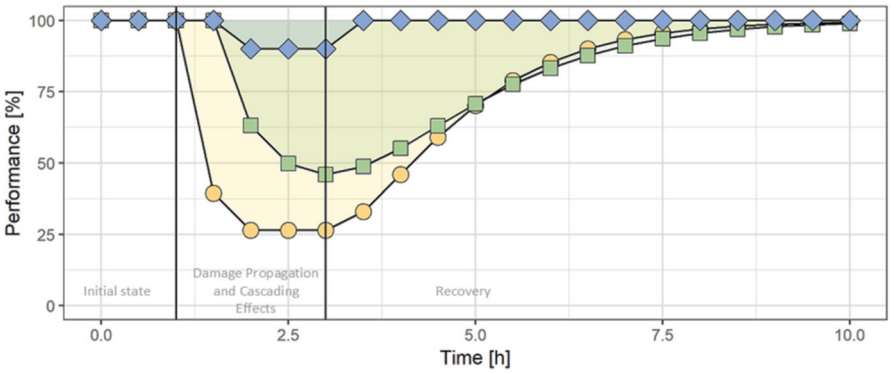

Fig. 2 Exemplary resilience curves for three coupled infrastructure networks, e.g. power (yellow), water (blue) and telecommunication (green), following an attack on the yellow network (first vertical line). Interdependencies result in cascading failures affecting other networks such as water supply and telecommunication. After node-dependent repair times, the network nodes are restored (second vertical line). The performance is defined by the percentage of operational nodes within the corresponding network. A single-valued resilience indicator can be derived from the integrated performance loss, represented by shaded areas between the curves and the ideal performance of 100%

Fig. 2. In general, it is also possible to observe cascading failures analogous to those featured in Fig. 2, in a quantum network. However, the interaction between the nodes of a quantum network—mediated by the dipole–dipole interactions—is physically different from the classical network. The quantum parallelism stemming from the ensuing multi-connectedness of a quantum network is the reason why QC might be useful in the resilience analysis, but a comprehensive comparison between cascading failures in quantum and classical networks can be the subject of future studies.

3 Implementation on a quantum computer

Here we provide some details of how to compute the state populations on IBM quantum hardware using the `qiskit` [27] interface, given the unitary extensions $\tilde{U}_n(t)$ of the Kraus operators. We illustrate the procedure for the case of a three-node system spanned by an effective five-dimensional Hilbert space, as described in Sect. 2.2.2.

First, we generate quantum circuits $C_n(t)$ corresponding to each unitary matrix $\tilde{U}_n(t)$. To that end, we use a built-in function of `qiskit.quantum_info` that transforms matrices into `Operator` objects acting on four qubits. The `Operator` objects are then decomposed into a sequence of basic quantum gates—a quantum circuit—by the `qiskit transpile` function. In all considered examples, rather deep circuits were generated (see Table 1). In Sect. 4, we discuss the effect of the circuit depth on the computational errors in more detail.

The transpilation must be repeated for each unitary $\tilde{U}_n(t)$ $(n = 0, \ldots, 4)$ and for each time step. As a result, a simulation of even a short, 50-time-step evolution of a three-node network with only one initial excitation and one damageable node yields

Table 1 Specification of quantum systems considered in this work

Name	Number of three-level nodes	Number of two-level nodes	dim $\mathcal{H}_{\text{eff}}$	size of $\tilde{U}_n$	Required # of qubits	Number of circuits per time step	Depth of circuit (max.)
QS-0-3	0	3	8	8×8	3	1	67
QS-1-0	1	0	3	8×8	3	3	67
QS-1-1	1	1	4	8×8	3	4	87
QS-1-2	1	2	5	16×16	4	5	399

Table 2 Error evaluation of the quantum systems introduced in Table 1

Name	Number of shots	Number of runs	Δ_{RMSE}	σ_{qc}
QS-0-3	4000	10	$1.17 \cdot 10^{-1}$	$3.74 \cdot 10^{-2}$
QS-1-0	10000	1	$1.36 \cdot 10^{-1}$	$6.75 \cdot 10^{-2}$
QS-1-1	10000	20	$1.33 \cdot 10^{-1}$	$7.13 \cdot 10^{-2}$
QS-1-2	10000	1	$2.35 \cdot 10^{-1}$	$1.72 \cdot 10^{-2}$

The deviation Δ_{RMSE} of the `IBM` hardware output from the analytical solution and the associated standard deviations σ_{qc} were extracted from a spline fit of the data points (see Fig. 3). Both Δ_{RMSE} and σ_{qc} were obtained by considering the states of the effective Hilbert space

250 circuits. This is close to 300, the maximum number of circuits that can be included in a single job on current IBM quantum computers.

After the circuits are generated, the populations $p_m(t)$ of the physical states

$$|m\rangle \in \{|0,0,0\rangle,\ |0,0,1\rangle,\ |0,1,0\rangle,\ |1,0,0\rangle,\ |2,0,0\rangle\}$$

can be computed by running the evolution of the circuits on quantum hardware and by projecting out the auxiliary dimensions followed by a measurement,

$$p_m(t) = \sum_{n=0}^{4} |\langle m| P_{\mathcal{H}} C_n(t) |\tilde{\varphi}_1\rangle|^2, \tag{14}$$

where $|\tilde{\varphi}_1\rangle = |1,0,0,0\rangle$ is the initial state in the extended four-qubit system and $P_{\mathcal{H}}$ performs a projection onto the effective Hilbert space. The populations $p_m(t)$ are approximated by the relative frequencies of the measured states $|m\rangle$ at the end of the circuit. We give the exact numbers of shots, i.e. the number of repetitions of quantum circuit executions, for each system in Table 2. It should be noted that the number of circuits would be larger for mixed initial states $\rho(0) = \sum_k c_k |\varphi_k\rangle\langle\varphi_k|$, since the evolution of every $|\varphi_k\rangle$ in the decomposition of $\rho(0)$ is represented by separate circuits. Additionally, the populations $p_m(t)$ in (14) are not normalized in general, as the different terms in the sum stem from different circuits. It is only in the case of zero noise (that is, on a quantum simulator) that the probabilities of all physical states sum up to unity.

4 Results

In this section, we report on our IBM QC experience, for four considered cases of increasing complexity. To benchmark these results, for each studied system we furnish the outcome of running the same circuits on a quantum simulator. We have checked that the latter results always coincide with the analytical results, which confirmed that the circuits were generated correctly and all deviations of the output of quantum computation from these results stem from the hardware's imperfections.

We set out with a system of three ideal (two-level) nodes connected by two links (QS-0-3). Although the defect levels in this case are absent, this example is instructive, since the unitary operator governing the network's dynamics has the same dimensions as the unitary dilations in two other cases also presented here: a single three-level node (QS-1-0) and a two-node network consisting of one three-level node coupled to a two-level node (QS-1-1). In particular, this enables us to gain some insights on how the depth of circuits depends on the size of a unitary and how this depth affects the scaling of errors on the quantum hardware. As a final example, we consider a network featuring a three-level node and two two-level nodes (QS-1-2).

A summary of the four setups is given in Table 1, while the details thereof and results are provided in the following subsections. All results were obtained from the IBM Q System One in Ehningen, henceforth called `ibm_ehningen`.

4.1 Coherent system

A network consisting of three qubits coupled by two links (setup QS-0-3 in Table 1) undergoes unitary dynamics governed by the Hamiltonians H_k and H_{int} (see Sect. 2.1 and Eq. (1)). The evolution of the network's state vector can be found for arbitrary parameters of the driving field and the dipole–dipole interactions. However, in order to make a smooth connection to other scenarios considered in the present contribution, we restrict ourselves to a simplified scenario of a single excitation stored in the network. We assume the initial state of the network to be $|0, 0, 1\rangle$. Hamiltonian (1) generates the unitary dynamics of the network; the corresponding 8×8 matrix can be evaluated analytically. In particular, the populations of the states $|1, 0, 0\rangle$, $|0, 1, 0\rangle$ and $|0, 0, 1\rangle$ are given, respectively, by $\sin^4(Jt/\sqrt{2})$, $\sin^2(J\sqrt{2}t)/2$ and $\cos^4(Jt/\sqrt{2})$; the population of all other states is zero.

The analytically obtained time-dependent populations are plotted along with the output of IBM quantum hardware in Fig. 3a. The hardware backend captures quite accurately the frequencies of the populations' oscillations (each population is a combination of two frequencies), but the overall mismatch between the exact and numerical results is significant (up to 25%), especially near the maxima. We attribute these errors to the considerable depth of the circuits (see Table 1).

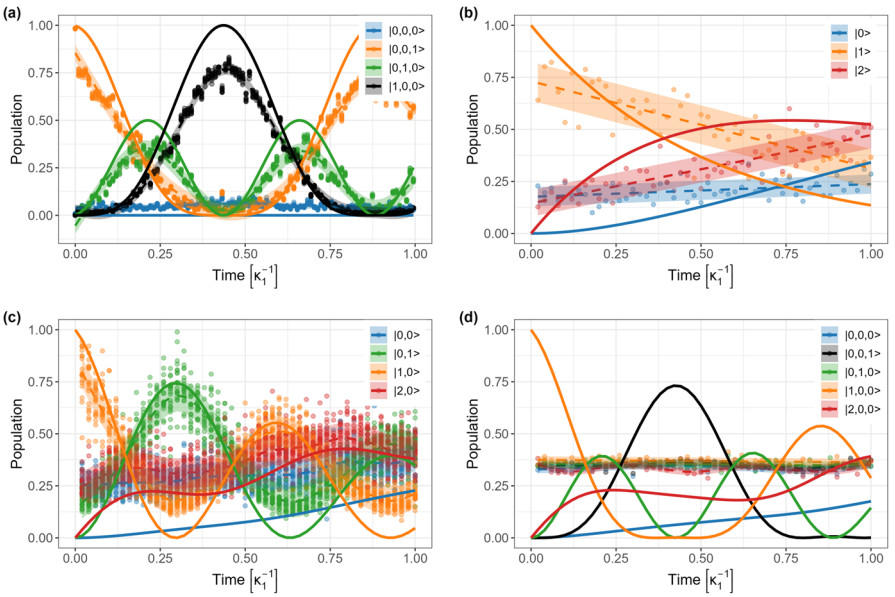

Fig. 3 Populations of the nodes' states (see the legends) vs. time (in units of κ_1^{-1}) obtained from the simulator (thin solid lines) and from `ibm_ehningen` (dots), where each dot represents the outcome of a single run. The latter results are averaged by a smoothing spline (dashed lines) with a cross-validation method [28] and the surrounding error bands show one standard deviation. The used parameters are $\kappa_2 = 0.4\kappa_1$, $J_{12} = J_{23} = J = 5\kappa_1$ and only states of the effective Hilbert spaces are shown. **a** QS-0-3: system of three ideal dipole-coupled nodes with two levels each. Here we also show the population of the ground state $|0, 0, 0\rangle$, in order to illustrate errors of the quantum hardware. **b** QS-1-0: one node with three levels. **c** QS-1-1: one dipole-coupled node with three levels to one node with two levels. **d** QS-1-2: one dipole-coupled node with three levels to two nodes with two levels each

4.2 Incoherent systems

4.2.1 Single three-level node

A single node (setup QS-1-0) represents the fundamental building block of our network, and it is also the simplest case for the implementation of the unitary dilation procedure [17, 26]. The Kraus operators and the unitary operators $\tilde{U}_n$ are given by 3×3 and 8×8 matrices, respectively. For the initially excited node, the time-dependent populations read ($\kappa_1 \neq \kappa_2$)

$$p_0(t) = \frac{\kappa_1 - e^{-\kappa_2 t}\kappa_1 + (e^{-\kappa_1 t} - 1)\kappa_2}{\kappa_1 - \kappa_2}, \tag{15a}$$

$$p_1(t) = e^{-\kappa_1 t}, \tag{15b}$$

$$p_2(t) = \frac{(e^{-\kappa_2 t} - e^{-\kappa_1 t})\kappa_1}{\kappa_1 - \kappa_2}, \tag{15c}$$

where $p_k(t)$ $(k = 0, 1, 2)$ is the population of level $|k\rangle$. At times $t \gg \kappa_1^{-1} \sim \kappa_2^{-1}$, $p_0 = 1$, $p_1 = p_2 = 0$, and the node can be re-initialized in state $|1\rangle$ by a laser pulse.

The output of `ibm_ehningen` in this case (see Fig. 3b) exhibits less similarity with the analytical results as for the three-node network of coupled qubits (see Sect. 4.1). The nonlinear evolution of the levels' populations, due to the exponential functions of time in Eq. (15), is represented by the output of the backend as almost straight lines; the scatter of the data is significant (see the wider error bands as compared to those in Fig. 3a), and at any time, there is a mismatch between the QC-generated and exact results. Only the general trend of the populations to increase or decrease with time is captured by the quantum hardware in the considered time interval. Although the dimension of the matrices representing the unitary operators $\tilde{U}_n$ and the depth of the corresponding circuits is the same as for three ideal nodes, we need three circuits at each time step (see Table 1), which explains larger systematic offsets and stronger scatter of the data points in this case.

4.2.2 One damageable and one ideal node

Now we consider a more complex case, where we combine the non-unitary dynamics of a single three-level node with the coherent exchange of excitation with another (two-level) node, via dipole–dipole coupling (setup QS-1-1). We recall that the state space for such a network is spanned by four state vectors $\{|0, 0\rangle, |0, 1\rangle, |1, 0\rangle, |2, 0\rangle\}$ (see also Sect. 2.2.2) and we chose $|1, 0\rangle$ as the initial state. In this case, as in the two previous cases, the unitary operators $\tilde{U}_n$ are given by 8×8 matrices, but their matrix elements are described by more complicated expressions, requiring deeper quantum circuits than in the previous cases (see Table 1).

The results for this system from `ibm_ehningen` (twenty repetitions for every circuit, with 10000 shots each) are shown in Fig. 3c, along with exact solutions. The levels' populations exhibit a behaviour that is characteristic of irreversible processes on top of the coherent evolution. For instance, we observe decaying oscillations of the populations and identify the characteristic time, $t_c \approx 0.3\kappa_1^{-1}$, of the excitation transfer between nodes 1 and 2, as half of the oscillation period in Fig. 3c.

The modulation frequencies of the curves are reproduced by `ibm_ehningen` rather accurately, but the data points exhibit much scatter, which results in large standard deviations (coloured bands) and the oscillation amplitudes of the smoothing splines are significantly less pronounced than for the exact results. The offset of the quantum computing results compared to the analytical results is similar as in the previous setup (QS-1-0).

4.2.3 One damageable and two ideal nodes

For setup QS-1-2, we chose the initial state of the network to be $|1, 0, 0\rangle$, where the first state of the three-node system refers to the damageable node, and found the Kraus operators governing the dynamics of this open quantum network. The matrices associated with unitary operators $\tilde{U}_n$ have dimensions 16×16, leading to a substantial increase in the circuits' depth up to 399 (see Table 1).

The results of quantum hardware in this case were dominated by systematic errors (see Fig. 3d). We tested QS-1-2 on different hardware back ends and the IBM Qasm-Simulator with a noise model that includes realistic effects of gate errors and readout errors, all leading to results similar to the `ibm_ehningen` results in Fig. 3d.

Summing all execution times on `ibm_ehningen` for this setup, excluding queue waiting time, leads to a total computation time of over 20 min, which is explained by the number of circuits required for a simulation of open quantum systems with the ansatz described in Sect. 2. This conflicts with our goal to use quantum computations to speed up classical simulations.

4.3 Error analysis

As follows from our discussion in Sect. 4.2 and from Fig. 3, our results on the quantum hardware show large variances and systematic deviations from the analytical solutions. In Table 2, a summary of the errors of the hardware results is provided for all setups, including also the number of shots per run and the number of repeated runs used to generate the results in the previous sections. To quantify the discrepancy between the quantum hardware's output (qc) and the exact results (qasm), we calculated the root mean square errors (RMSE) that are averaged over all states in the effective Hilbert space,

$$\Delta_{\mathrm{RMSE}} = \frac{1}{N_s}\sum_{s=1}^{N_s}\sqrt{\frac{1}{N_t}\sum_{n=1}^{N_t}\left(p_s^{\mathrm{qasm}}(t_n) - p_s^{\mathrm{qc}}(t_n)\right)^2}, \tag{16}$$

where s labels the relevant states (i.e. with theoretical nonzero populations during the circuit's execution), N_s is the total number of such states, t_n are the evaluated times and N_t is the total number of time steps. As derived from Eq. (14), $p_s^{\mathrm{qasm}}(t)$ is the population of state s at time t computed by the QASM simulator (exact result) and $p_s^{\mathrm{qc}}(t)$ is the value of the populations obtained from the spline fit of the `ibm_ehningen` results. The mean of the standard deviations σ_{qc} was obtained analogously for the quantum computer results. Table 2 shows the comparison of both error metrics for all systems studied, together with additional information on the number of shots and runs, respectively.

With increasing complexity of the system, larger standard deviations σ_{qc} were observed. However, this does not hold for system QS-1-2, where we find a smaller variance for each state's population. In fact, all populations are approximately constant in time and are almost the same in magnitude, which is close to $5/16$, i.e. the value for a uniform distribution, since these results were obtained using five circuits acting on four qubits. The errors Δ_{RMSE} for QS-0-3, QS-1-0 and QS-1-1 are on a comparable scale, which is expected, as all three systems use the same number of qubits and feature a similar circuit depth (see Table 1). For QS-1-2, a significantly larger value is obtained for Δ_{RMSE}, due to the complete loss of correlation between the hardware output and the dynamical behaviour of the state's populations.

As we argued in Sect. 4.2.3, our method suffers from long execution times, mainly due to the number of circuits needed for a complete simulation. To keep the computation time as short as possible, larger time steps can be used, or the number of

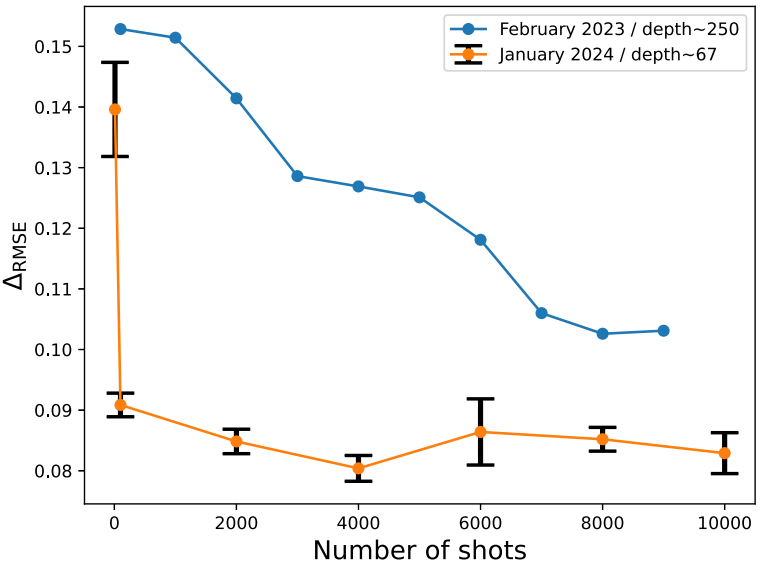

Fig. 4 Root mean square error, averaged over all states in the three-qubit Hilbert space, vs number of shots. The curves show two iterations of the setup QS-0-3, conducted in February 2023 (blue line) and in January 2024 (orange line). In the latter case, the experiment was repeated 10 times and orange dots and black error bars indicate the mean values and the standard deviations of these 10 runs, respectively

shots can be optimized in the sense of effectiveness, i.e. minimized while keeping sufficient measurement statistics. To test this latter strategy, we evaluated Δ_{RMSE} for the setup QS-0-3 on `ibm_ehningen`, averaged over all single node states involved in the dynamics for different numbers of shots, see Fig. 4. This analysis was carried out in February 2023 and in January 2024, after system upgrades of `ibm_ehningen` had been announced. While, in 2023, the reduction of Δ_{RMSE} prevailed up to the largest number of shots (blue line), the 2024 results (orange line) rapidly stabilized to a well-defined output level within the computed standard deviations (black error bars) that were obtained from ten runs of system QS-0-3 for each tested number of shots. The overall 12–40% reduction of Δ_{RMSE} in 2024 compared to 2023 can be explained by an improvement in the transpilation process, leading to much shorter circuits with mean depths of 67 in 2024 compared to depths of around 200 in 2023. The results in Fig. 4 suggest that, with the upgraded system, 4000 shots provide sufficient statistics for a system like QS-0-3.

5 Conclusion

We conceived a small quantum network model of critical infrastructure, with the main goal of establishing how efficiently this quantum system can be simulated on a gate-based quantum computer. The distinctive feature of our approach is that we describe nodes of the network by three-level open quantum systems, with two levels representing intact nodes which mediate the functionality of the network, and a third

defect level serving to mimic a node's incoherent damage and repair. This made our approach very intuitive, enabling us to directly incorporate into our model basic properties of the nodes of critical infrastructure—their vulnerability, i.e. their possibility to be damaged, as well as their ability to recover. Furthermore, we can import the well-established formalism of Lindblad-type quantum master equations to model the evolution of the network's state. A second attractive feature of our model is a linear scaling of the number of required qubits with the nodes of the quantum network.

However, the implementation of our method on quantum hardware requires knowledge of an operator-sum representation of the master equation in analytical form, which was here accomplished for small networks containing up to three nodes, where only one node includes the defect level. A further challenge which we could not entirely overcome is the large depths of circuits that were produced by the transpilation function from `qiskit`. This led to very large systematic errors and to unreliable results of our quantum computations. Complete breakdown of the IBM computation was observed when considering a three-level node coupled to two two-level nodes. On the other hand, qualitatively correct results could be achieved for systems with one three-level node and up to one additional two-level node. The modulation frequencies of the state populations were rather accurately reproduced on the quantum hardware, for an open quantum system with a four-dimensional effective Hilbert space.

In the future, these investigations may be taken further into different directions: it will be interesting to investigate whether error mitigation techniques [29] allow for a reduction of the computation errors. Further optimization potential regarding computation time is also indicated by our error analysis. As the field of quantum circuit optimization has been rapidly developing [30], efficient algorithms that automatically reduce the circuit depth, output by the `qiskit` transpilation function, might become available, which will allow us to study larger systems. To further increase the size of potentially studied systems, an automatized numerical derivation of the Kraus operators at each time step seems suggestive. Furthermore, to actually identify the most resilient network topologies the method of quantum trajectories [18] appears as a complementary strategy to the here employed master equation approach, since it allows to mimic a network's real-time evolution in terms of intact and failing nodes, at each point in time.

Appendix A The Kraus operators

A.1 QS-1-1

For this two-node system, there are four Kraus operators $M_n(t)$, each of which is represented in the basis $\{|0,0\rangle, |0,1\rangle, |1,0\rangle, |2,0\rangle\}$ by 4×4 matrices. The explicit expressions for the four nonzero elements of operator $M_1(t)$ read:

$$(M_1)_{14}(t) = \left(\frac{8J^2\kappa_2 e^{-\kappa_1 t}}{w^2(\kappa_1 - 2\kappa_2)} + \frac{\kappa_1\kappa_2 e^{-\kappa_1 t}\left(\left(\kappa_1\kappa_2 - 2J^2\right)\cos(wt) + \kappa_2 w \sin(wt)\right)}{w^2\left(J^2 + \kappa_2(\kappa_2 - \kappa_1)\right)}\right.$$

$$+\frac{\kappa_1 e^{-2\kappa_2 t}\left(J^2+\kappa_2(2\kappa_2-k_1)\right)}{(2\kappa_2-\kappa_1)\left(J^2+\kappa_2(\kappa_2-\kappa_1)\right)}+1\Bigg)^{1/2}, \tag{A1}$$

$$(M_1)_{23}(t)=\frac{2iJe^{-\kappa_1 t/2}(\cos(wt)-1)(4J^2-\kappa_1(\kappa_1\cos(wt)+w\sin(wt))^{1/2}}{w\left(\frac{4J^2}{(\kappa_1-w\cot(\frac{wt}{2}))^2}+1\right)^{1/2}(\kappa_1(\cos(wt)-1)+w\sin(wt))}, \tag{A2}$$

$$(M_1)_{33}(t)=\frac{e^{-\kappa_1 t/2}\left(4J^2-\kappa_1(\kappa_1\cos(wt)+w\sin(wt))\right)^{1/2}}{w}\left(\frac{4J^2(\cos(wt)-1)^2}{(\kappa_1(\cos(wt)-1)+w\sin(wt))^2}+1\right)^{-1/2}, \tag{A3}$$

$$\begin{aligned}(M_1)_{42}(t)=\Bigg(&-\frac{4J^2\kappa_1 e^{-\kappa_1 t}}{w^2(\kappa_1-2\kappa_2)}+\frac{i\left(2J^2\kappa_1(-2\kappa_1+iw)-\kappa_1^3(-\kappa_1+iw)\right)e^{-(\kappa_1-iw)t}}{w^3(\kappa_1-2\kappa_2-iw)}\\&+\frac{i\left(2J^2\kappa_1(2\kappa_1+iw)-\kappa_1^3(\kappa_1+iw)\right)e^{-(\kappa_1+iw)t}}{w^3(\kappa_1-2\kappa_2+iw)}\\&+\frac{\kappa_1 e^{-2\kappa_2 t}\left(J^2+\kappa_2(2\kappa_2-\kappa_1)\right)}{(\kappa_1-2\kappa_2)\left(J^2+\kappa_2(\kappa_2-\kappa_1)\right)}\Bigg)^{1/2},\end{aligned} \tag{A4}$$

with $w:=\sqrt{4J^2-\kappa_1^2}$. The operator $M_1(t)$ fully determines nonzero matrix elements of the remaining Kraus operators:

$$(M_1)_{14}=(M_2)_{11}=(M_3)_{13}=(M_4)_{12}, \tag{A5a}$$
$$(M_1)_{23}=(M_2)_{22}=(M_3)_{24}=(M_4)_{21}, \tag{A5b}$$
$$(M_1)_{33}=(M_2)_{32}=(M_3)_{34}=(M_4)_{31}, \tag{A5c}$$
$$(M_1)_{42}=(M_2)_{44}=(M_3)_{41}=(M_4)_{43}. \tag{A5d}$$

A.2 QS-1-2

We compute the Kraus operators $M_n(t)$ $(n=1,\ldots,5)$ for this three-node system spanned by states $\{|0,0,0\rangle,\ |0,0,1\rangle,\ |0,1,0\rangle,\ |1,0,0\rangle,\ |2,0,0\rangle\}$ in two steps. First, from the master equation we generated the 25×25 matrix $\boldsymbol{A}$ governing the evolution of its 25 matrix elements. The eigenvalues, $\vec{\lambda}=(\lambda_1,\ldots,\lambda_{25})^T$, and eigenvectors, $\boldsymbol{V}=(\vec{v}_1^T\ldots\vec{v}_{25}^T)$, of $\boldsymbol{A}$ can be found exactly for arbitrary values of J, κ_1 and κ_2, because $\boldsymbol{A}$ is sparse and its diagonalization requires solving of cubic or lower-order algebraic equations. Then the evolution of the density matrix $\rho(t)$ can be found from the equation $\boldsymbol{V}\boldsymbol{D}\boldsymbol{V}^{-1}|\rho_0\rangle\rangle$, with $\boldsymbol{D}=\mathrm{diag}(e^{\lambda_1 t},\ldots,e^{\lambda_{25}t})$ and $|\rho_0\rangle\rangle=(\rho_{1,1}(0),\rho_{1,2}(0),\ldots,\rho_{25,25}(0))^T$ the initial density matrix vector.

Second, the eigensystem of the density matrix $\rho(t)$ can be evaluated at $t > 0$ (in symbolic form) at fixed, but arbitrary numerical values of parameters J, κ_1 and κ_2. The resulting expressions are very lengthy and we do not provide them here. We only mention that the nonzero matrix elements of $M_1(t)$ fully determine all Kraus operators, via identities analogous to (A5):

$$(M_1)_{14} = (M_2)_{13} = (M_3)_{11} = (M_4)_{12} = (M_5)_{15}, \tag{A6a}$$
$$(M_1)_{22} = (M_2)_{25} = (M_3)_{24} = (M_4)_{23} = (M_5)_{21}, \tag{A6b}$$
$$(M_1)_{32} = (M_2)_{35} = (M_3)_{34} = (M_4)_{33} = (M_5)_{31}, \tag{A6c}$$
$$(M_1)_{42} = (M_2)_{45} = (M_3)_{44} = (M_4)_{43} = (M_5)_{41}, \tag{A6d}$$
$$(M_1)_{55} = (M_2)_{54} = (M_3)_{53} = (M_4)_{51} = (M_5)_{52}. \tag{A6e}$$

Acknowledgements This work was funded by the projects EFFEKTIF and SEQUOIA End-to-End funded by the Baden-Württemberg Ministry of the Economy, Labour and Housing.

Author Contributions C.B.H and V.S. wrote the main manuscript text. A.K.J. and M.F.K. prepared Figs. 2, 3 and 4 and wrote the main part of the error analysis chapter. A.K.J., C.K., A.S. and M.F.K. provided background information on resilience analysis and contributed to the introduction. A.B. gave feedback on all applied methods and interpretation of the results. All authors reviewed the manuscript.

Funding Open Access funding enabled and organized by Projekt DEAL.

Data Availability The data that support the findings of this study are available from the corresponding author upon reasonable request.

Declarations

Conflict of interest The authors declare no Conflict of interest.

References

1. Balakrishnan, S., Cassottana, B.: InfraRisk: an open-source simulation platform for resilience analysis in interconnected power-water-transport networks. Sustain. Cities Soc. **83**, 103963 (2022)
2. Mühlhofer, E., Koks, E.E., Kropf, C.M., Sansavini, G., Bresch, D.N.: A generalized natural hazard risk modelling framework for infrastructure failure cascades. Reliab. Eng. Syst. Saf. **234**, 109194 (2023)
3. Huang, Z., Wang, C., Ruj, S., Stojmenovic, M., Nayak, A.: Modeling cascading failures in smart power grid using interdependent complex networks and percolation theory. In: 2013 IEEE 8th Conference on Industrial Electronics and Applications (ICIEA), pp. 1023–1028. IEEE (2013)

4. Parandehgheibi, M., Modiano, E., Hay, D.: Mitigating cascading failures in interdependent power grids and communication networks. In: 2014 IEEE International Conference on Smart Grid Communications (SmartGridComm), pp. 242–247. IEEE (2014)
5. Fehling-Kaschek, M., Miller, N., Haab, G., Faist, K., Stolz, A., Häring, I., Neri, A., Celozzi, G., Sanchez, J., Valera, J.: Risk and resilience assessment and improvement in the telecommunication industry. In: Proceedings of the 30th European Safety and Reliability Conference and the 15th Probabilistic Safety Assessment and Management Conference (PSAM15). ESREL (2020)
6. Feynman, R.P.: Simulating physics with computers. Int. J. Theor. Phys. **21**(6), 467–488 (1982). https://doi.org/10.1007/BF02650179
7. Shor, P.W.: Polynomial-time algorithms for prime factorization and discrete logarithms on a quantum computer. SIAM J. Comput. **26**(5), 1484–1509 (1997). https://doi.org/10.1137/S0097539795293172
8. Grover, L.K.: A fast quantum mechanical algorithm for database search. In: Proceedings of the Twenty-Eighth Annual ACM Symposium on Theory of Computing. STOC '96, pp. 212–219. Association for Computing Machinery, New York, NY, USA (1996). https://doi.org/10.1145/237814.237866
9. Ehningen, I.: IBMQ. https://quantum.ibm.com/
10. Scholak, T., Wellens, T., Buchleitner, A.: The optimization topography of exciton transport. EPL (Europhys. Lett.) **96**(1), 10001 (2011). https://doi.org/10.1209/0295-5075/96/10001
11. Scholak, T., Melo, F., Wellens, T., Mintert, F., Buchleitner, A.: Efficient and coherent excitation transfer across disordered molecular networks. Phys. Rev. E **83**, 021912 (2011). https://doi.org/10.1103/PhysRevE.83.021912
12. Scholak, T., Wellens, T., Buchleitner, A.: Spectral backbone of excitation transport in ultracold Rydberg gases. Phys. Rev. A **90**, 063415 (2014). https://doi.org/10.1103/PhysRevA.90.063415
13. Nielsen, M.A., Chuang, I.L.: Quantum Comput. Quantum Inf., p. 205. Cambridge University Press, Cambridge (2000)
14. Sauter, T., Neuhauser, W., Blatt, R., Toschek, P.E.: Observation of quantum jumps. Phys. Rev. Lett. **57**, 1696–1698 (1986). https://doi.org/10.1103/PhysRevLett.57.1696
15. Bergquist, J.C., Hulet, R.G., Itano, W.M., Wineland, D.J.: Observation of quantum jumps in a single atom. Phys. Rev. Lett. **57**, 1699–1702 (1986). https://doi.org/10.1103/PhysRevLett.57.1699
16. Breuer, H.P., Petruccione, F.: The Theory of Open Quantum Systems. Oxford University Press, Oxford (2002)
17. Hu, Z., Xia, R., Kais, S.: A quantum algorithm for evolving open quantum dynamics on quantum computing devices. Sci. Rep. **10**(1), 3301 (2020). https://doi.org/10.1038/s41598-020-60321-x
18. Endo, S., Sun, J., Li, Y., Benjamin, S.C., Yuan, X.: Variational quantum simulation of general processes. Phys. Rev. Lett. **125**, 010501 (2020). https://doi.org/10.1103/PhysRevLett.125.010501
19. García-Pérez, G., Rossi, M.A.C., Maniscalco, S.: IBM Q experience as a versatile experimental testbed for simulating open quantum systems. npj Quantum Information **6**(1), 1 (2020). https://doi.org/10.1038/s41534-019-0235-y
20. Schlimgen, A.W., Head-Marsden, K., Sager, L.M., Narang, P., Mazziotti, D.A.: Quantum simulation of open quantum systems using a unitary decomposition of operators. Phys. Rev. Lett. **127**, 270503 (2021). https://doi.org/10.1103/PhysRevLett.127.270503
21. Schlimgen, A.W., Head-Marsden, K., Sager, L.M., Narang, P., Mazziotti, D.A.: Quantum simulation of the Lindblad equation using a unitary decomposition of operators. Phys. Rev. Res. **4**, 023216 (2022). https://doi.org/10.1103/PhysRevResearch.4.023216
22. Hu, Z., Head-Marsden, K., Mazziotti, D.A., Narang, P., Kais, S.: A general quantum algorithm for open quantum dynamics demonstrated with the Fenna-Matthews-Olson complex. Quantum **6**, 726 (2022). https://doi.org/10.22331/q-2022-05-30-726
23. Sweke, R., Sinayskiy, I., Bernard, D., Petruccione, F.: Universal simulation of Markovian open quantum systems. Phys. Rev. A **91**, 062308 (2015). https://doi.org/10.1103/PhysRevA.91.062308
24. Tong, D.M., Kwek, L.C., Oh, C.H., Chen, J.-L., Ma, L.: Operator-sum representation of time-dependent density operators and its applications. Phys. Rev. A **69**, 054102 (2004). https://doi.org/10.1103/PhysRevA.69.054102
25. Nakazato, H., Hida, Y., Yuasa, K., Militello, B., Napoli, A., Messina, A.: Solution of the Lindblad equation in the Kraus representation. Phys. Rev. A **74**, 062113 (2006). https://doi.org/10.1103/PhysRevA.74.062113
26. Levy, E., Shalit, O.M.: Dilation theory in finite dimensions: the possible, the impossible and the unknown. Rocky Mt. J. Math. **44**(1), 203–221 (2014). https://doi.org/10.1216/RMJ-2014-44-1-203

27. Qiskit contributors: Qiskit: An Open-Source Framework for Quantum Computing (2023). https://doi.org/10.5281/zenodo.2573505
28. Helwig, N.E.: Npreg: Nonparametric Regression Via Smoothing Splines. (2022). R package version 1.0-9. https://CRAN.R-project.org/package=npreg
29. Cai, Z., Babbush, R., Benjamin, S.C., Endo, S., Huggins, W.J., Li, Y., McClean, J.R., O'Brien, T.E.: Quantum error mitigation. Rev. Mod. Phys. **95**, 045005 (2023). https://doi.org/10.1103/RevModPhys.95.045005
30. Karuppasamy, K., Puram, V., Johnson, S., Thomas, J.P.: A comprehensive review of quantum circuit optimization: current trends and future directions. Quantum Rep. (2025). https://doi.org/10.3390/quantum7010002